Tamaki, K., Suyehiro, K., Allan, J., McWilliams, M., et al., 1992
Proceedings of the Ocean Drilling Program, Scientific Results, Vol. 127/128, Pt. 2

47. GEOCHEMISTRY AND ISOTOPIC COMPOSITION OF VOLCANIC ROCKS FROM THE YAMATO BASIN: HOLE 794D, SEA OF JAPAN[1]

André Pouclet[2] and Hervé Bellon[3]

ABSTRACT

The Yamato Basin basement in the Sea of Japan was drilled below the sediment pile during Legs 127 and 128. Two superposed volcanic complexes are distinguished. The upper complex consists of continental tholeiite sills dated around 20–18 Ma and attributed to the rifting stage of the backarc basin. The lower complex consists of backarc basin basalts probably intruded below the upper complex during the spreading stage. Trace-element compositions and Sr and Nd isotopic signatures may be explained by mixing of at least two end members with a very small addition of crustal and subducted sediment component. Thus, upwelling of mantle diapir occurred during the rifting stage. Contribution of the depleted mantle increased in the spreading stage. The Neogene magmatic history of the Japan Sea is reviewed in the light of the ODP new data.

INTRODUCTION

During Leg 128 of the Ocean Drilling Program in the Sea of Japan, highest priority was assigned to recovery of basement rocks, which record the earliest phases of the backarc basin evolution. At Site 794, in the northern Yamato Basin, igneous rocks were recovered at the end of the sedimentary pile that partly represent the acoustic basement on seismic reflection profiles. This site was initially drilled during Leg 127 (Tamaki, Pisciotto, Allan, et al., 1990) and revisited during Leg 128 (Ingle, Suyehiro, von Breymann, et al., 1990) to drill deeper (Fig. 1). A total of 191.1 m of stacked dolerite and basalt sills, and rare interbedded sediments was penetrated from 542.2 to 733.5 m below seafloor (mbsf).

LITHOLOGY

Lithologic units were distinguished on the basis of petrography and on-board X-ray fluorescence (XRF) analyses, and from the logging record which differentiated sedimentary zones and resistive massive igneous strata. New shore-based chemical analyses have been performed on selected samples, and the logging record was re-examined (wireline logs of the Lamont-Doherty Geological Observatory). Figure 2 presents the revised lithologic distinction.

Seven igneous units were recognized (Units 1 to 7); only one sediment unit was recovered (Unit VI). Unit 1 is a thick laccolith of plagioclase-phyric dolerite. Units 2 and 3 are determined to be olivine-dolerite sills. Sedimentary Unit VI is a marine clayey siltstone; it includes a 10-cm-thick layer of hyaloclastite shards attesting to a proximal underwater eruption. Unit 4 is a doleritic basalt shallow sill. Units 5–7 consist of olivine-rich dolerite sills. In terms of seismic stratigraphy (Tamaki, Pisciotto, Allan, et al., 1990), the lowermost highly reflective interval is recorded between 543 mbsf and 710 mbsf (Units 1–6), below the stratified sedimentary column and above the unstratified acoustically opaque zone. The interlayered volcanic and sedimentary rocks represent this latter interval, and the lower volcanic unit may belong to the true basement. Thus, the igneous rocks recovered at Site 794 constitute the uppermost crust of the Yamato Basin.

GEOCHEMISTRY

Many of the igneous rocks recovered during drilling at Site 794 have been analyzed onboard by X-ray fluorescence (XRF) method (Tamaki, Pisciotto, Allan, et al., 1990; Ingle, Suyehiro, von Breymann et al., 1990). These data are used to exhibit the geochemical variations on Figure 2. We have selected 16 samples (Table 1) for shore-based chemical investigations: inductively coupled plasma spectrometry (ICP) and inductively coupled plasma with mass spectrometry (ICP-MS). The results allow us to test the accuracy of the onboard data by duplicating some analyses, and to obtain additional data (rare earth elements, Nb, Th, U). As a whole, except for cerium, the XRF analyses are adequate. Thus, the distinction among units is maintained. Table 2 presents the major and trace elements analyses by ICP of the selected samples labeled per core number and representative of Units 1–7.

Effect of Alteration

The major-element oxides are recalculated water free with $Fe_2O_3/FeO = 0.15$ because many rocks are highly altered, as indicated by the high loss on ignition. Glass and groundmass are completely converted to secondary minerals: smectites, chlorites, and sideromelane. All the olivine is replaced by smectites and serpentine. Plagioclase and pyroxene microcrysts may be partly altered. In addition, the lower part of the pile is invaded by hydrothermal veins of saponite, chlorite, calcite, and pyrite (Proust et al., this volume). As a consequence, the major-element composition was modified by leaching or enrichment of mobile elements. By comparing the relative correlation of elements with loss on ignition (LOI), MgO, SiO_2, and K_2O show a positive correlation, and CaO and FeO, a negative correlation. Post-eruption Mg-enrichment is evidenced by the composition of spinels, which allow determination of the original magmatic Mg/Fe ratio (Allan, this volume). It is also suggested that some large-ion lithophile elements were mobile during alteration: Rb, K, and probably Ba and Sr. The rare earth elements (REE), the high-field-strength elements (HFSE) and Th seem to be relatively immobile (Pearce and Cann, 1973; Saunders and Tarney, 1984). Detailed investigations of Allan and Gorton (this volume) show that the HFSE and the REE are relatively immobile in fresher samples but that Ce, Yb, Lu, Y, Rb, and Sr have been redistributed in altered samples where LOI exceeds 3.5%.

Geochemical Distinction

All the lavas are classified as tholeiites with respect to their mineralogy and chemistry. Nevertheless, preliminary investigations clearly

[1] Tamaki, K., Suyehiro, K., Allan, J., McWilliams, M., et al., 1992. *Proc. ODP, Sci. Results,* 127/128, Pt. 2: College Station, TX (Ocean Drilling Program).
[2] Géotectonique et Pétrologie, Faculté des Sciences, Université d'Orléans, BP 6759, 45067 Orléans cedex 2, France.
[3] Laboratoire de Géochimie et de Géochronologie. URA 1278 CNRS et GDR 910. Université de Bretagne Occidentale, 29287 Brest cedex, France.

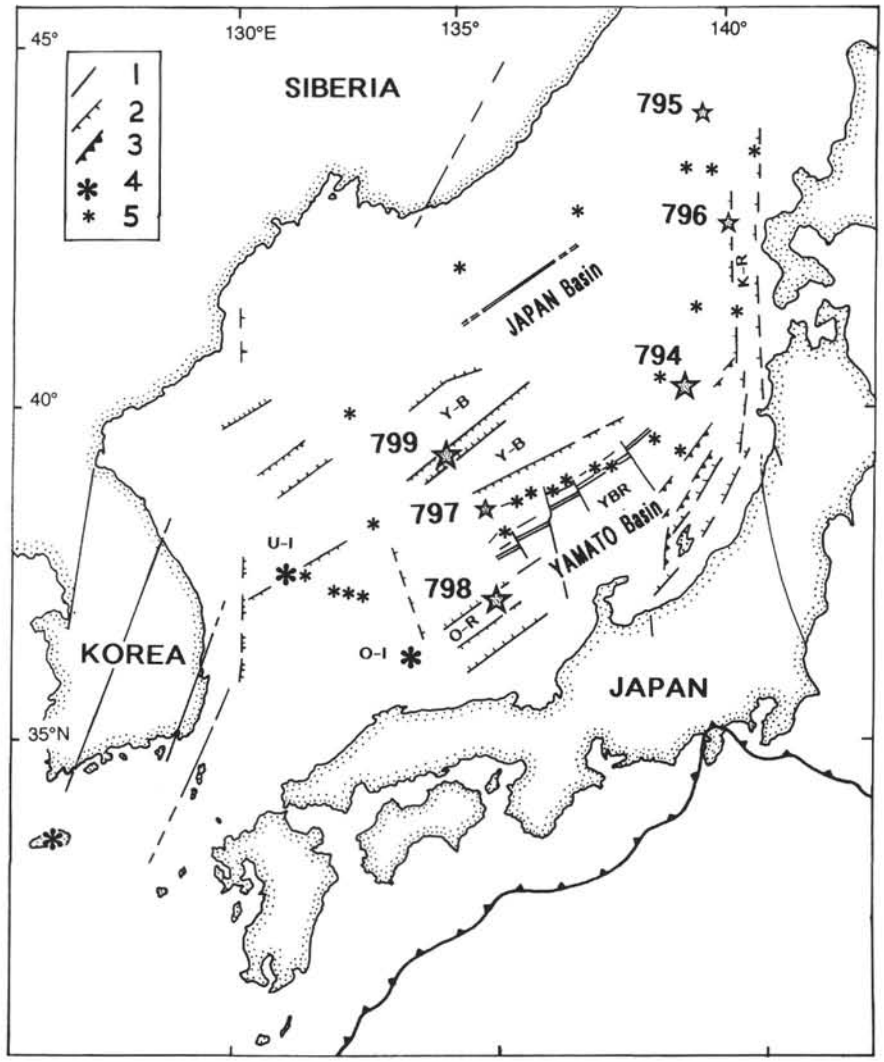

Figure 1. Location and structural setting of the ODP Sites in the Japan Sea: Legs 127 (Sites 794, 795, 796, and 797) and 128 (Sites 794, 798, and 799). 1, strike-slip faults; 2, normal faults; 3, thrusts and subduction zone; 4, volcanic islands; 5, seamounts; double solid lines, spreading axis; K-R, Okushiri Ridge; O-I, Oki Islands; O-R, Oki Ridge; U-I, Ulleung Island; Y-B, Yamato Bank; YBR, Yamato Basin Ridge (Kimura et al., 1987).

showed that the units may have distinctive chemical compositions (Ingle, Suyehiro, von Breymann, et al., 1990; Fig. 2). The chemical distinction is carried out by using the less mobile incompatible elements: REE, Nb, Th, Y, and Zr. In the binary diagrams (Fig. 3) the rocks are distributed in three groups. Table 3 presents their averaged discriminant features. Group 1 includes Units 1, 2, and 3. Composition is Nb-, La-, Th-, and Ba-rich, and Y-poor. This group is defined as the Upper Volcanic Complex (UVC). Group 2 corresponds to Unit 4; it is depleted in incompatible element content: Nb, Th, Y, Yb, and Zr. It is labeled as the Middle Volcanic Unit (MVU). Group 3 includes Units 5, 6, and 7. Composition is relatively Nb-, La-, Th-, and Ba-poor, and Y-, Yb-, and Ti-rich. This group is defined as the Lower Volcanic Complex (LVC).

The chondrite-normalized REE patterns (Evensen et al.,1978) for representative samples from the three groups exhibit clear distinctions (Fig. 4A). The UVC shows a light rare-earth element (LREE) enrichment. The MVU is very slightly LREE-enriched. The LVC has a flatter pattern. The chondrite-normalized ratios La/Yb are, respectively, 3.31, 2.08, and 1.19. N-MORB- (Pearce, 1982) and mantle- (Wood et al., 1979) normalized amount of incompatible elements are used for geochemical distinctions (Fig. 4B and 4C). However, Sr-, K-, Rb-, and Ba-contents may be questionable in the most hydrated samples (Table 2, Cores 11R and 9R) because of the mobility of these elements during alteration. As a whole, the UVC is depleted in heavy rare-earth elements (HREE) and Ti, and enriched in large-ion lithophile elements (LILE). In contrast, the LVC is enriched in HFSE and depleted in LILE. The MVU is depleted in both HFSE and LILE, but some negative and positive anomalies (Rb, Ba, K, Sr) are due to alteration. Taking into account the alteration effect, the MVU may be close to the UVC magma.

Magmatic Characterization

Correlation diagrams and normalized diagrams suggest that the UVC and the LVC originated from different sources. Assignment of magmatic series is used to determine the paleotectonic environment of volcanics.

The LILE enrichment of the UVC characterizes arc volcanic rocks. But there are no negative anomalies of Nb and Zr, no LREE depletion relative to N-MORB composition, and no flat trend of the

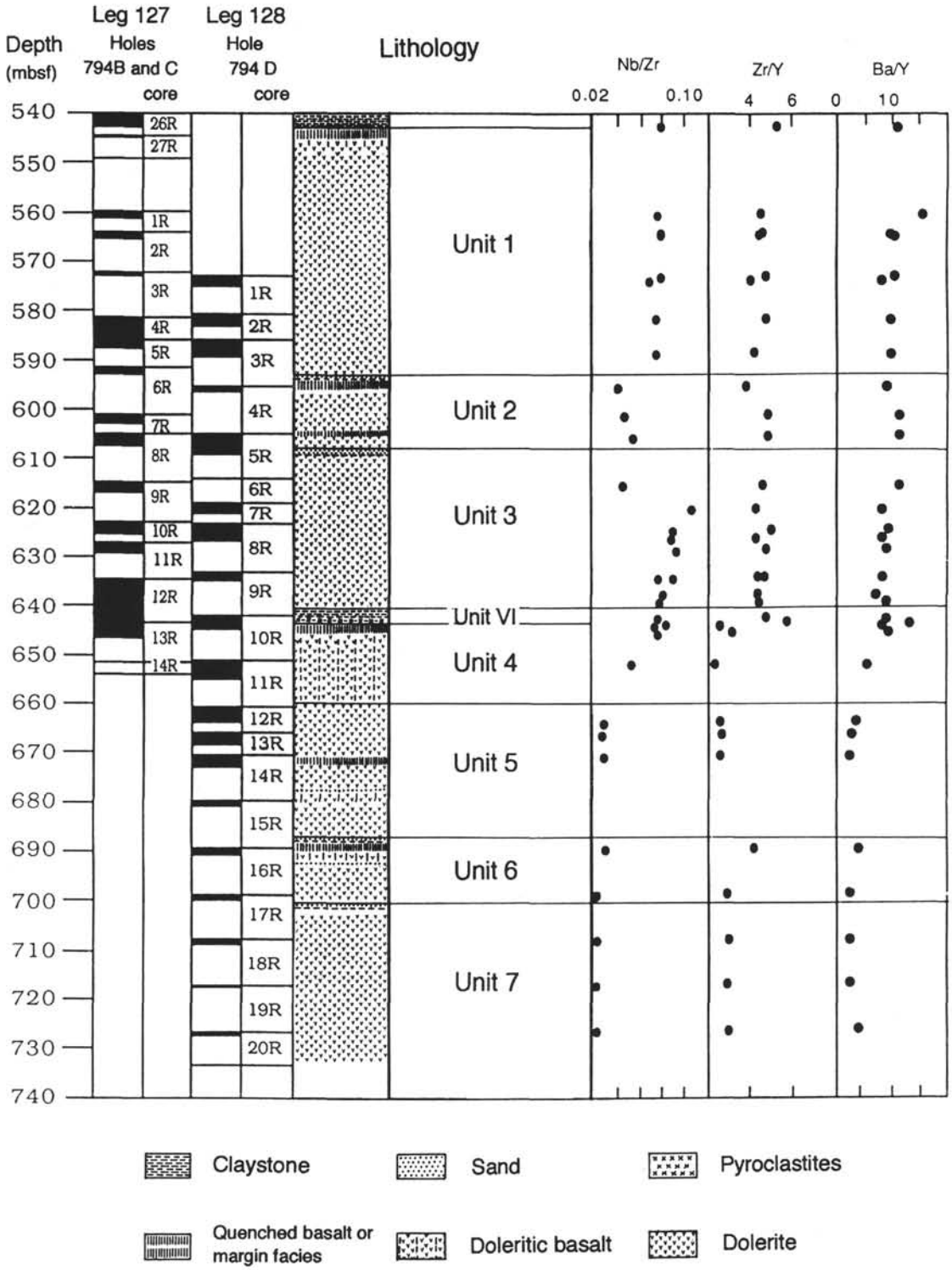

Figure 2. Core recovery of igneous rocks at Site 794 (Ingle, Suyehiro, von Breymann, et al., 1990). Lithology, revised unit boundaries, and geochemical variations.

HFSE. Low values of the La/Nb ratio (1–1.26) preclude a subduction-related origin (Thompson et al., 1983). In fact the UVC composition is similar to that of intraplate tholeiitic volcanics, except for lower amounts of Nb and Ti. Exactly the same composition characterizes the early to middle Miocene basalts of the Akita-Yamagata rift zone in northwest Japan (Tsuchiya, 1990).

Trace-element patterns of LVC are close to those of enriched MORB. LILE and HFSE contents of the LVC are similar to MORB composition with slight depletion in Nb and slight enrichment in Sr, Rb and Th. Some of this enrichment may be due to secondary alteration, but the Th content is primary (Saunders and Tarney, 1984). The MORB affinity is evidenced in Figure 3 (similar Y/Zr and Nb/Zr

Table 1. Core, section, and interval location of analyzed samples.

Sample	Core and section	Interval (cm)
1R	1R-1	96–101
3R	3R-3	89–94
4R	4R-1	32–37
7R	7R-2	8–10
8R	8R-2	126–130
9R	9R-2	16–20
10R	10R-2	70–74
11R	11R-1	89–95
12R	12R-3	36–40
13R	13R-1	81–84
14R	14R-1	81–84
16R	16R-1	67–70
17R	17R-1	97–100
18R	18R-1	44–47
19R	19R-1	11–14
20R	20R-1	20–23

ratios). Compared to the back-arc basalt compositions in the Zr-normalized multi-element plots of Saunders and Tarney (1984), the LVC shows low positive anomaly of Th and low negative anomaly of Nb. A comparable, nearly flat pattern characterizes the Parece Vela Basin basalts (Saunders and Tarney, 1984). We concluded that a smaller proportion of subducted components is involved in the genesis of the LVC basalt.

MVU has the same Th and Nb contents as LVC, but it is more depleted in HREE and HFSE. Compared to UVC, lower incompatible element contents and higher Cr contents would be explained by a less evolved magma.

In considering discriminant diagrams of Pearce and Cann (1973), and of Meschede (1986) (Fig. 5A, 5B, and 5C), UVC overlaps the intraplate (WPB), the MORB, and the active margin basalt (CAB, LKT) fields. MVU plots in the Low-K Tholeiitic (LKT) or in the MORB fields. LVC plots in the MORB and in the Ocean Floor Basalt (OFB) fields. That only demonstrates the affinity between LVC and MORB. The recent ternary diagram La/Y/Nb (Cabanis and Lecolle, 1989) yields more interesting information (Fig. 5D). The composition of the UVC is close to that of continental tholeiites and continental initial rifting tholeiites, according to averages of Holm (1985), whereas the LVC composition plots in the back-arc basin basalt field between IAT and N-MORB fields. The composition of MVU is intermediate. That is in good agreement with the normalized spidergrams.

Petrogenic Interpretations

According to the Zr/Y vs. Zr diagram of Pearce and Norry (1979) (Fig. 6), UVC basalt originated from slightly enriched mantle source. LVC basalt plots on a distinct petrogenic pathway from non-enriched to slightly depleted source. In the Th/Yb vs. Nb/17/Yb covariation diagram adapted from Pearce (1982) (Fig. 7), the Yamato substratum lava compositions are close to the MORB-primordial mantle-intraplate

Table 2. Major- and trace-element chemical composition of igneous rocks. Inductively coupled plasma spectrometry, X-ray fluorescence spectrometry (Ba, Cr, Cu, Ni, Rb, Sr), and inductively coupled plasma and mass spectrometry for Samples 3R, 9R, 11R, and 13R (REE, Th, U).

	Unit 1		Unit 2		Unit 3		Unit 4			Unit 5		Unit 6			Unit 7	
Sample	1R	3R	4R	7R	8R	9R	10R	11R	12R	13R	14R	16R	17R	18R	19R	20R
SiO_2	50.81	51.11	52.58	51.57	51.13	51.43	51.38	50.11	49.37	49.08	50.53	51.97	49.92	50.03	50.47	48.44
TiO_2	1.30	1.28	1.06	1.43	1.29	1.53	1.09	1.18	1.75	1.62	1.67	1.74	1.57	1.68	1.57	1.56
Al_2O_3	19.14	18.01	17.05	16.20	16.05	16.66	16.14	16.29	15.65	15.56	15.06	19.34	17.91	18.04	18.02	17.18
Fe_2O_3	1.21	1.21	1.02	1.08	1.14	1.13	1.18	1.22	1.44	1.42	1.42	0.99	1.17	1.07	1.16	1.29
FeO	8.08	8.03	6.79	7.22	7.63	7.52	7.85	8.20	9.59	9.47	9.40	6.63	7.79	7.11	7.69	8.57
MnO	0.13	0.12	0.23	0.12	0.12	0.14	0.14	0.16	0.18	0.18	0.21	0.21	0.27	0.25	0.16	0.18
MgO	5.96	6.24	10.64	10.19	10.72	10.51	13.83	11.44	7.34	8.28	6.79	7.09	7.20	6.95	6.48	8.84
CaO	8.85	9.61	5.41	8.15	7.86	7.20	2.75	8.19	10.91	10.85	11.00	7.73	10.78	10.90	10.84	10.47
Na_2O	3.74	3.59	3.54	3.27	3.21	3.06	2.50	2.84	3.50	3.26	3.53	3.66	3.00	3.52	3.23	3.08
K_2O	0.58	0.59	1.51	0.56	0.66	0.59	2.98	0.25	0.13	0.15	0.21	0.35	0.21	0.21	0.20	0.22
P_2O_5	0.20	0.21	0.17	0.21	0.19	0.23	0.16	0.13	0.15	0.13	0.17	0.28	0.17	0.24	0.18	0.19
TOTAL	100.00	100.00	100.00	100.00	100.00	100.00	100.00	100.00	100.00	100.00	100.00	100.00	100.00	100.00	100.00	100.00
LOI	2.80	2.51	6.50	3.31	6.45	5.34	5.98	6.41	1.76	1.52	1.98	5.59	3.29	3.52	3.05	2.48
La		7.7				8.5		3.7		4.4				5.0		4.2
Ce		17.7				18.4		8.8		11.4				11.9		9.9
Pr		2.3				2.4		1.2		1.7						
Nd		10.3				10.3		5.7		9.2				11.8		9.5
Sm		2.8				2.9		1.7		3.2				4.0		3.3
Eu		1.1				1.1		0.8		1.2				1.4		1.1
Gd		3.3				3.5		2.2		4.2				4.7		3.6
Tb		0.5				0.6		0.4		0.7						
Dy		3.3				3.6		2.4		5.0				5.2		4.2
Ho		0.7				0.7		0.5		1.0						
Er		1.9				2.0		1.4		2.9				2.9		2.4
Tm		0.3				0.3		0.2		0.4						
Yb		1.6				1.7		1.2		2.5				2.8		2.2
Lu		0.2				0.2		0.2		0.3				0.3		0.3
Ba	122	154	143	133	129	121	89	57	48	21	11	58	10	6	12	53
Cr	47	79	358	216	313	266	341	377	288	324	311	329	283	319	312	291
Cu	30	34	39	56	46	51	18	54	58	63	63	55	61	74	60	56
Nb	6.0	6.1	4.0	11.0	8.0	8.6	3.0	2.5	3.0	2.8	3.0	4.0	2.0	3.0	2.0	2.0
Ni	12	21	182	88	159	126	128	147	82	129	117	113	108	124	137	124
Rb	6.0	7.0	9.0	4.0	7.0	5.0	13.0	0.4	1.0	3.0	4.0	5.0	3.0	3.0	3.0	2.0
Sr	395	370	238	279	246	277	171	277	196	194	191	263	181	200	185	173
Th		0.8				1.0		0.3		0.3						
U		0.2				0.3		0.0		0.0						
V	272	238	257	289	252	278	250	256	271	245	284	278	255	281	232	234
Y	20	20	21	22	21	20	15	16	34	31	33	29	31	33	29	28
Zn	28	49	57	36	44	49	28	47	75	85	91	108	77	83	81	53
Zr	85	90	85	100	93	99	41	41	96	90	95	131	97	107	92	92

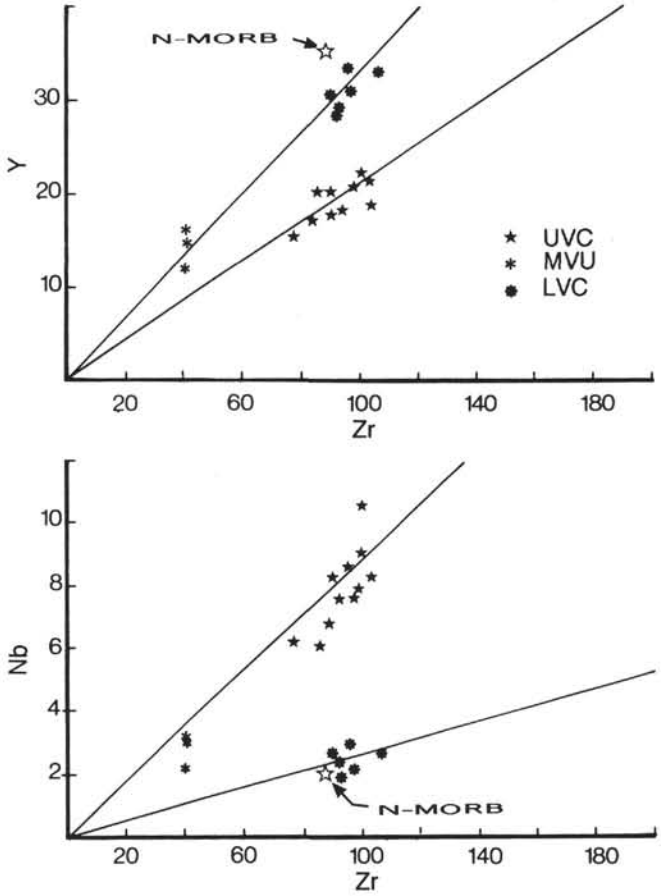

Figure 3. Covariation diagrams in the Y-, Nb-, and Zr-incompatible elements. UVC, upper volcanic complex; MVU, middle volcanic unit; LVC, lower volcanic complex. N-MORB composition after Pearce (1982).

Table 3. Discriminant trace-element contents, means of upper volcanic complex (UVC), middle volcanic unit (MVU), and lower volcanic complex (LVC) basalts.

	UVC	MVU	LVC
La	8.1	3.7	4.6
Yb	1.7	1.2	2.5
[a]La/Yb	3.31	2.08	1.19
Ba	138	73	30
Nb	8.5	2.8	2.5
Th	0.9	0.3	0.3
TiO_2	1.25	1.14	1.60
Y	20	14	31
Zr	90	41	94
[b]Th/Nb	0.80	0.77	0.69
[b]Nb/Zr	1.38	1.09	0.56
[c]Th/Ce	2.49	1.70	1.32
[c]Zr/Y	1.58	0.85	0.97

[a] Chondrite-normalized ratio
[b] Mantle-normalized ratio
[c] MORB-normalized ratio

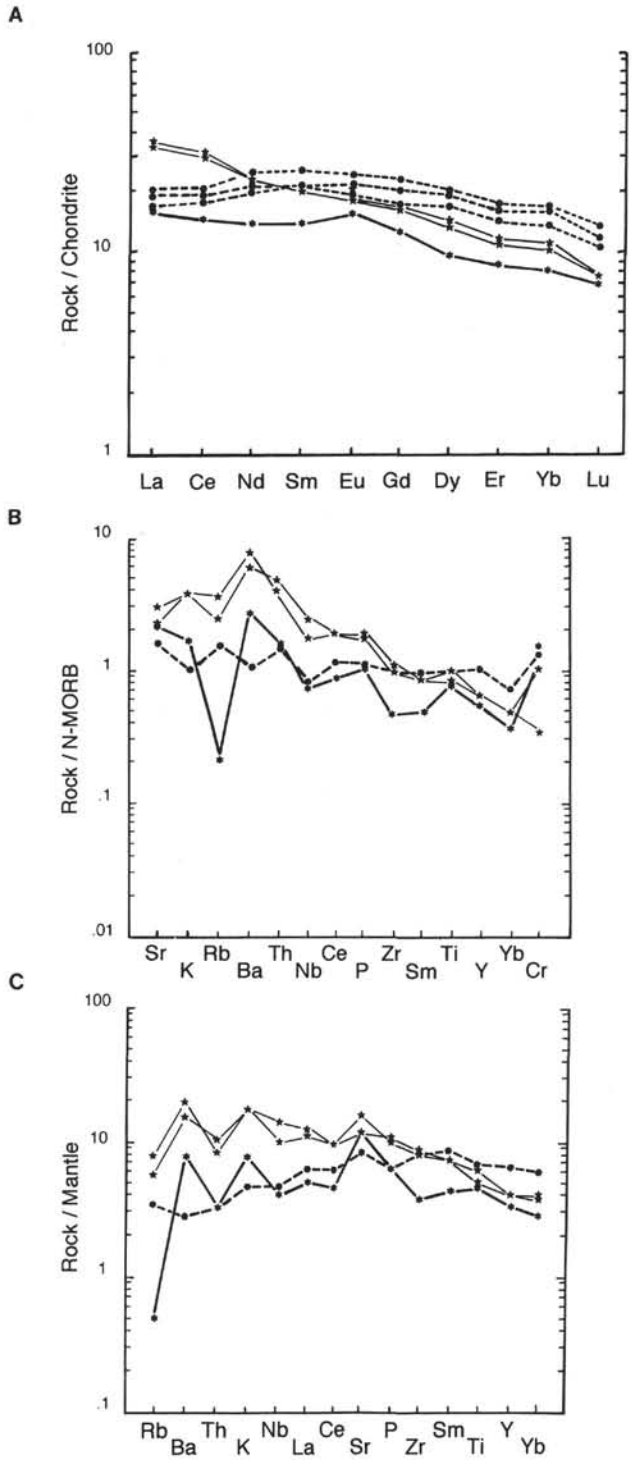

Figure 4. Spidergrams. **A.** Chondrite-normalized REE pattern (Evensen et al., 1978). **B.** N-MORB normalized hygromagmaphile elements (Pearce, 1982). **C.** Primordial mantle-normalized hygromagmaphile elements (Woods et al., 1979). Same symbols as for Figure 3.

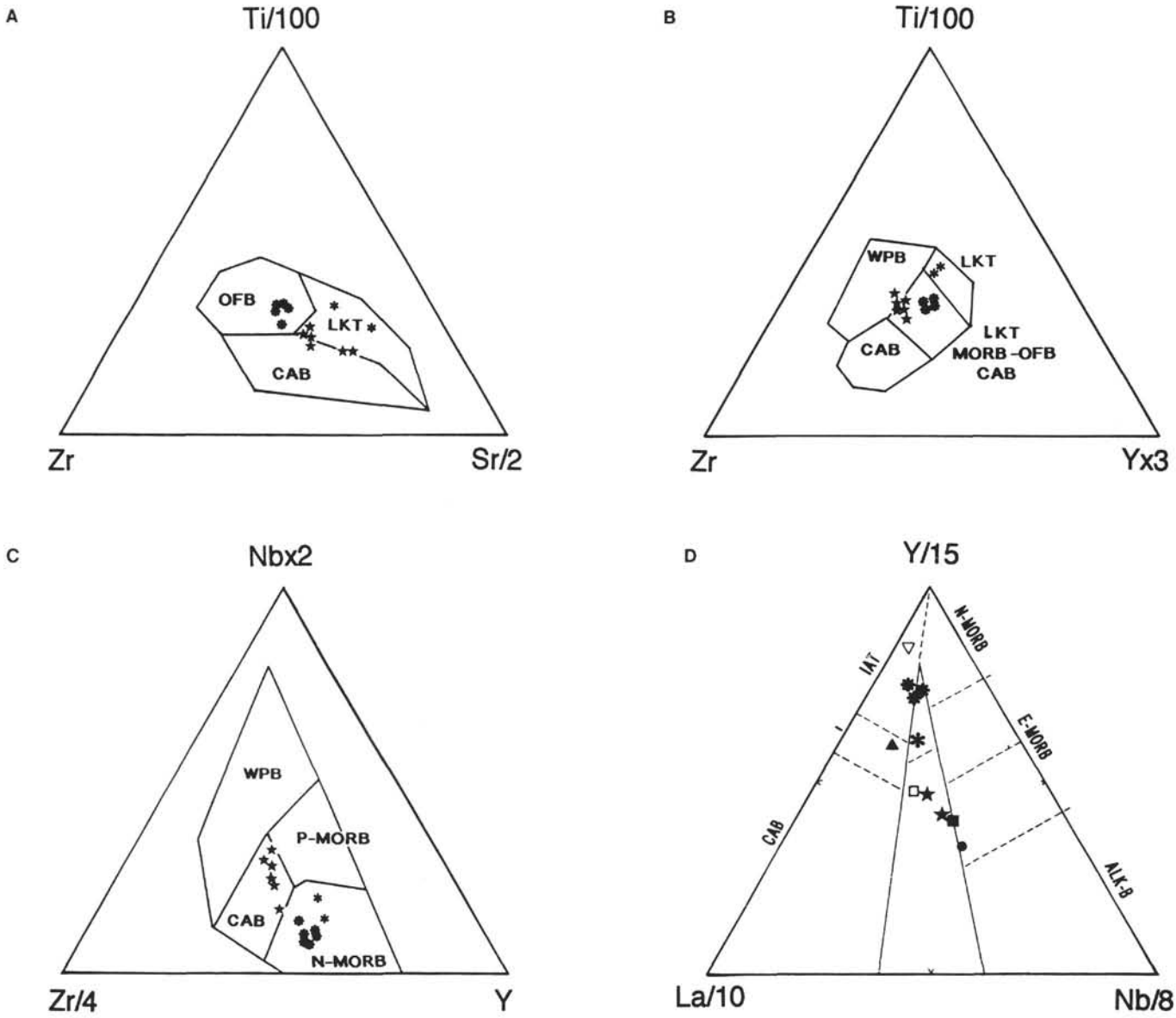

Figure 5. Triangular discriminant diagrams. **A.** Zr-Ti/100-Sr/2. **B.** Zr-Ti/100-Y×3. **C.** Zr/4-Nb×2-Y. **D.** La/10-Y/15-Nb/8. ALK-B, intraplate alkaline basalt; CAB, calc-alkaline basalt; IAT, island arc tholeiite; LKT, low-K tholeiite; MORB, mid-ocean ridge basalt: N, normal; E, enriched; P, plume-related; OFB, ocean floor basalt; WPB, within-plate basalt. Same symbols as for Figure 3. Solid square, initial rifting tholeiites in continental settings; open square, continental tholeiites; solid triangle, calc-alkaline lavas of Japan; open inverted triangle, arc tholeiites of Japan. A and B, after Pearce and Cann (1973). C, after Meschede (1986). D, after Cabanis and Lecolle (1989).

basalt (WPB) mixing array with a small addition of Th. This is also the case for basalts of the Akita-Yamagata rift zone (Tsuchiya, 1990).

UVC originated from a weakly enriched source, and LVC from a slightly depleted source. The UVC to LVC evolution trend is parallel to the MORB-WPB array. This evolution may reflect various mixing of two enriched and depleted sources with slight Th crustal or subducted sediment contamination. No strong variation in contamination (Th content) is observed.

K/Ar RADIOMETRIC MEASUREMENTS

Eight lavas have been selected for ^{40}K-^{40}Ar isotopic dating: three from the UVC (Table 2, Cores 1R, 3R, and 8R), one from the MVU (Table 2, Core 11R), and four from the LVC (Table 2, Cores 12R, 13R, 14R, and 20R). The rocks are moderately to highly altered as shown by the loss on ignition and the secondary-minerals modal content (Ingle, Suyehiro, von Breymann, et al., 1990). UVC and MVU lavas suffered seawater alteration, the extent of which is controlled by grain size and thickness of igneous units. Secondary minerals developed at the expense of glass and fine-grained groundmass of the margins of intrusive bodies. Similar but less-important seawater alteration concerns LVC lavas; however, an additional hydrothermal alteration affected the lower units.

Experimental Procedure

Analyses were performed on whole-rock samples (0.5–0.16 mm in size fraction) and were complemented with analyses of separated plagioclases (between 250- and 63 µm) from two rocks: Cores 13R and 20R. Argon was extracted from 1 g of whole rock and from 0.2

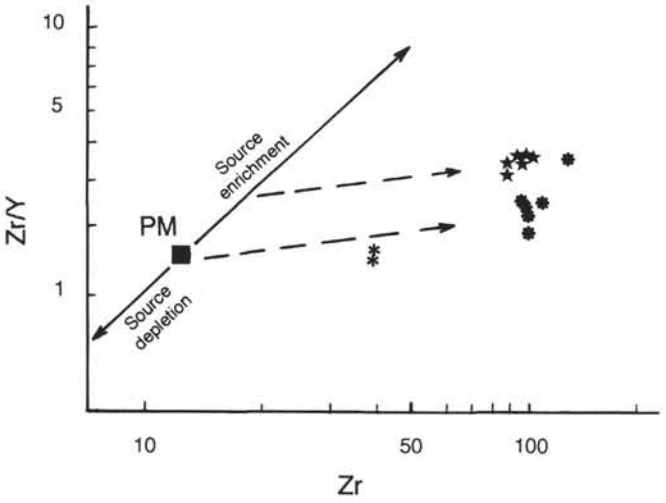

Figure 6. Zr/Y vs. Zr diagram after Pearce and Norry (1979). Same symbols as for Figure 3. PM, primordial mantle.

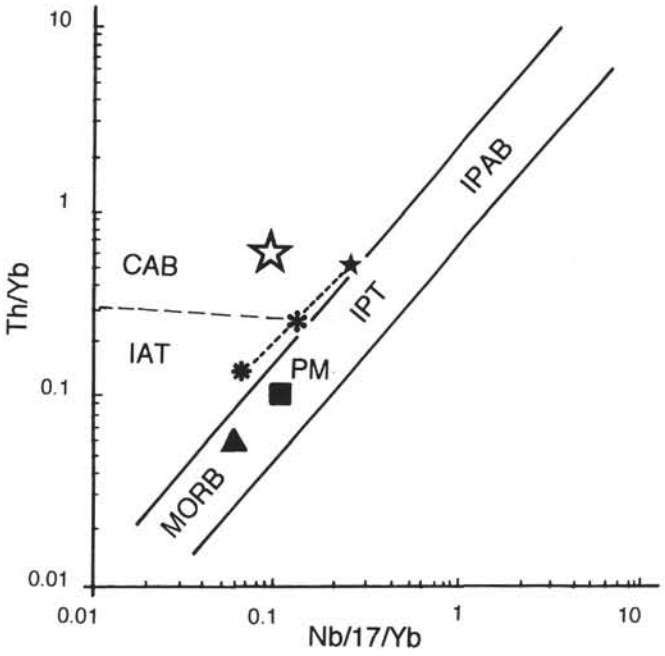

Figure 7. Nb/17/Yb vs. Th/Yb covariation diagram adapted from Pearce (1982). Nb is used instead of Ta; the ratio Nb/Ta = 17 is consistent with the analyses of Nb and Ta in similar rocks by Allan and Gorton (this volume). IPAB, intraplate alkaline basalt; IPT, intraplate tholeiite; MORB, mid-ocean ridge basalt. Same symbols as for Figure 3. Star, calc-alkaline lavas of Japan; solid square, primordial mantle (PM); solid triangle, MORB normalizing value.

to 0.4 g of plagioclase under high vacuum by induction heating; it was cleaned of active gases by a series of titanium furnaces. A final purification by two Al-Zr getters was done just before and during the mass spectrometric analysis of argon. The isotopic composition of argon in each sample was measured with reference to the isotopic composition of Ar in air run in the same way after each measurement, to correct for mass discrimination effects. Radiogenic ^{40}Ar was determined by isotope dilution using an original procedure described in Bellon et al. (1981), where the ^{38}Ar spike is buried as ions in an aluminium foil target. Each target with a precise ^{38}Ar content of 1.40×10^{-7} cm^3 (s = 1%) regularly calibrated with the standard sample glauconite GI-O (Cassignol et al., 1977) was added to the sample at the time of weighing.

Isotopic Concentrations and Age Calculations

Radiogenic ^{40}Ar ($^{40}Ar_R$), ^{36}Ar, and the ratio of radiogenic ^{40}Ar to total ^{40}Ar (radiogenic + atmospheric Ar, $\%^{40}Ar_R$) are listed in Table 4. Concentrations have been corrected for nonradiogenic Ar of atmospheric composition linked to the wrapping aluminum foil of the sample (typical concentration is 3.5×10^{-10} cm^3 for ^{36}Ar) and to the blank line that varies for a set of nine samples from 7×10^{-10} cm^3 (in the first under vacuum extraction) to 1.2×10^{-10} cm^3 (in the ninth extraction) for ^{36}Ar. As a consequence, corrected values of ^{36}Ar concentrations are characteristic of each sample and are representative of atmospheric contamination during crystallization or inheritance by secondary processes.

Ages are calculated using the constants recommended by Steiger and Jäger (1977). Errors are estimates of the standard deviation of precision (1 s) calculated using the error equation proposed by Mahood and Drake (1982), which includes an error term for the mass spectrometer discrimination.

Isotopic Dates

Calculated ages are presented in Table 4. The two whole-rock "oldest" ages, 35.5 and 44.1 Ma (Cores 20R and 11R) must be discarded because their ^{36}Ar values are very high compared to the ^{36}Ar values determined for the other LVC lavas. These high values may reflect a strong secondary contamination by a source having an isotopic argon composition slightly higher than the isotopic composition of air. This secondary process may have occurred during fluid circulations responsible for the large development of alteration. A similar process may have occurred for Core 8R. However, if we

Table 4. K-Ar radiometric measurements. WR, whole rock; PL, plagioclase. See text for comments.

Sample	Age (Ma)	^{40}Ar (10^{-7}cm^3/g)	^{36}Ar (10^{-9}cm^3/g)	^{40}Ar %	K_2O %	LOI %	Alt. %	Gm. %
1R	(WR) 20.61± 2.88	4.07	7.58	15.4	0.61	2.80	20	55
3R	(WR) 18.12± 1.22	3.76	3.18	28.5	0.64	2.51	15	50
	(WR) 18.33± 1.27	3.80	3.81	28.0				
8R	(WR) 23.65± 4.96	5.80	14.99	10.7	0.69	6.45	55	80
11R	(WR) 44.13± 8.63	3.60	9.49	11.4	0.25	6.41	50	70
12R	(WR) 14.12± 1.35	0.64	0.79	21.4	0.14	1.76	12	10
13R	(PL) 20.25± 3.67	0.43	1.10	11.7	0.069			
	(WR) 16.35± 0.51	1.11	0.34	52.4	0.21	1.52	15	10
	(WR) 16.75± 0.48	1.14	0.30	56.0	0.21			
14R	(WR) 15.24± 0.89	1.18	0.84	32.1	0.24	1.98	15	10
20R	(PL) 14.48± 3.83	0.31	1.18	8.3	0.07			
	(WR) 35.51± 9.12	2.54	8.86	8.8	0.22	2.48	20	10

consider samples at the same state of alteration, the UVC lavas are richer in ^{36}Ar than the LVC lavas.

Crucial discussion arises about the true age of the emplacement of the two volcanic complexes. Indeed, isotopic ages measured on the UVC samples range between 20.61 and 18.12 Ma. Because the younger age is from the sample with the lowest ^{36}Ar content, we think that this age is the most probable. Isotopic ages measured on the LVC samples having the lower ^{36}Ar contents range between 16.75 and 14.12 Ma. But we must keep in mind that the LVC lavas are invaded by hydrothermal veins. Results given by the plagioclases remain more problematic because of too little ^{40}Ar- and K-contents. The Core 20R mineral separated from a hydrothermally altered rock yields an age of 14.18 Ma, much younger than the whole rock (35.51 Ma) but with a large error. The Core 13R plagioclase yields an age of 20.25 Ma, apparently older than the age of the whole rock (16.50 Ma).

Concurrently, five ^{40}Ar-^{39}Ar measurements have been performed with UVC and LVC samples giving relatively good plateau ages (Kaneoka et al., this volume): Core 3R = 20.6 ± 0.6 Ma (1 s), Core 8R = 20.0 ± 2.0 Ma, Core 15R = 19.9 ± 0.7 Ma, Core 17R = 20.9 ± 0.9 Ma, and Core 20R = 21.2 ± 0.8 Ma. The data concerning the UVC lavas are in a good agreement with our results. We conclude that the upper volcanic complex is dated between 22 and 17 Ma. But the LVC age measurements are significantly older than our results, and in the age range of the UVC. It is highly probable that the LVC lavas have suffered a loss of radiogenic argon during hydrothermal alteration. Figure 8 shows a comparison between K-Ar (this work) and Ar-Ar age measurements (Kaneoka et al., this volume). Finally, the relative timing of the emplacement of the two volcanic complexes cannot be judged.

Sr AND Nd ISOTOPIC COMPOSITIONS

Sr and Nd isotopic compositions were determined for some Hole 794D igneous rocks. High seawater alteration is a strong limitation for measurements of the magmatic compositions, especially for the Sr isotopes. We selected two samples of the UVC, one of the MVU, and three of the LVC (Table 5). The $^{87}Sr/^{86}Sr$ ratio has a short range from enriched (MVU: 0.704928) to depleted composition (UVC: 0.704341–0.704162; LVC: 0.704339–0.704060). The $^{143}Nd/^{144}Nd$ ratio ranges from low, to moderate positive values (MVU: 0.512724; UVC: 0.512789–0.512820; LVC: 0.512918–0.512992). Compositions lie above the mantle array in Figure 9. Some data are added for comparison: dredged lavas from the Yamato Basin seamounts and floor of Miocene age (Nakamura and Tatsumoto in Kaneoka, 1990), Miocene-Pliocene lavas from the backarc side of the Japan arc (Nohda et al., 1988), early Miocene andesites, and Quaternary volcanic island alkaline basalt of the Korea Margin (Pouclet et al., unpublished data).

High Sr isotope ratio of the MVU doleritic basalt is due to seawater alteration (high LOI and strong negative anomaly of Rb). This may be also the case for some LVC dolerites that have suffered hydrothermal contamination; their initial magmatic signature is probably closer to the prevalent mantle composition (PM, Zindler and Hart, 1986) as demonstrated by the Yamato Basin dredged samples and the Japan backarc side samples.

We conclude that UVC originated from a weakly depleted source, and that LVC came from a little more depleted source compared to bulk earth (BE). These results are in a good agreement with the geochemical data.

Kaneoka (1990) suggested that high Sr isotope ratios of the Yamato lavas may be explained by incorporation of continental crustal material during magma extrusion. This would have affected the content of lithophile elements, particularly Th. Such a Th enrichment is not too important in the Site 794 lavas and seawater alteration is a more likely candidate for Sr isotopic anomalies. A continuous shift from enriched to depleted mantle sources as a function of time is observed by Nohda et al. (1988) in basalts from the backarc side of the Japan arc, the early Miocene lavas showing an enriched signature. This is not contradictory to our data. Lead isotopic compositions of Legs 127 and 128 igneous rocks (B. Cousens, pers. comm., 1990; Cousens and Allan, this volume) seems to preclude any participation of the EM I component (enriched mantle I, Walvis, subcontinental mantle) at the expense of

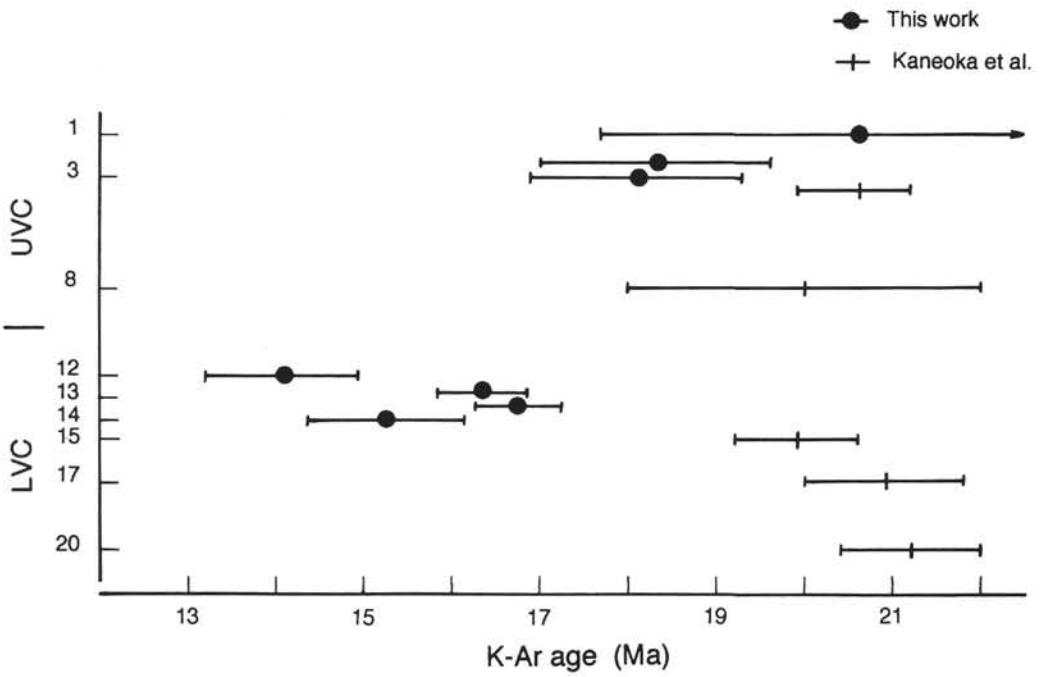

Figure 8. K-Ar age dating per units compared to Ar-Ar measurements of Kaneoka et al. (this volume). Errors are 2-sigma. UVC, upper volcanic complex; LVC, lower volcanic complex.

Table 5. Sr and Nd isotope data.

	3R	9R	11R	13R	18R	20R
Rb	7	5	0.4	3	3	2
Sr	370	277	277	194	200	173
Age (Ma)	19	(19)	(19)	(16.5)	(16.5)	(16.5)
$^{87}Sr/^{86}Sr_p$	0.704177 ± 0.000010	0.704356 ± 0.000012	0.704929 ± 0.000010	0.704350 ± 0.000012	0.704070 ± 0.000012	0.704114 ± 0.000011
$^{87}Sr/^{86}Sr_i$	0.704162	0.704342	0.704928	0.704340	0.704060	0.704104
$^{143}Nd/^{144}Nd$	0.512820 ± 0.000011	0.512789 ± 0.000012	0.512724 ± 0.000012	0.512944 ± 0.000011	0.512918 ± 0.000011	0.512992 ± 0.000016
[a]E Sr	–4.80	–2.24	+6.08	–2.27	–6.24	–5.62
[a]E Nd	+3.86	+3.26	+1.99	+6.28	+5.77	+7.22

Note: Estimated ages from K/Ar measurements: p, present-day measured ratios; i, initial ratios. Ratios are normalized to $^{86}Sr/^{88}Sr = 0.1194$ and to $^{146}Nd/^{144}Nd = 0.7219$. Values for NBS standard: $^{87}Sr/^{86}Sr = 0.71025 \pm 4$ (2σ) and La Jolla standard = 0.51186±3 (2σ).

[a]I Sr = 0.7045 and I Nd = 0.512622, present-day undifferentiated mantle reservoir (Wasserburg et al., 1981). Samples being young, no corrections for Nd-decay are needed.

the EM II component (enriched mantle II, Society, subducted oceanic sediments, or deep mantle source) (Zindler and Hart, 1986).

One may expect that the magma source of the Yamato basement basalts included at least two end members: EM II and DM (N-MORB source depleted mantle) (Fig. 9). Continental tholeiites of the upper volcanic complex resulted in dual contribution of EM II and DM. Backarc basin tholeiites of the lower volcanic complex gained increasing contribution from DM reservoir. If magma genesis implies upwelling of a mantle diapir, this may be associated with the convective asthenospheric motion mechanically induced by subducting slab (Uyeda, 1986). Then, increased mixing with entrained surrounding depleted upper mantle may have occurred in the backarc basin spreading stage, linked to eastward retreat of the subducting slab.

DISCUSSION AND CONCLUSION

Yamato Basin Rifting and Spreading

The uppermost crust of the Yamato Basin at Site 794 includes two superposed volcanic complexes of distinct magmatic composition. Igneous rocks consist of tholeiite sills intruded at the base of the sediment pile. The upper complex lavas are classified as tholeiites of continental initial rifting tectonic affiliation. The trace-element and

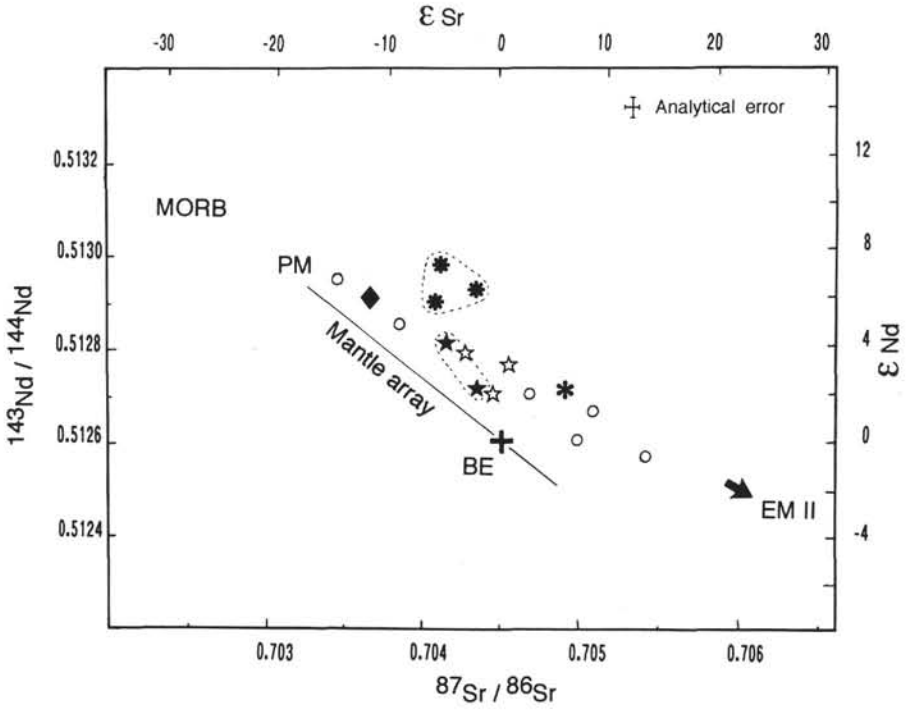

Figure 9. Sr and Nd isotope ratios. PM, prevalent mantle (Zindler and Hart, 1986). MORB: N-MORB depleted mantle (DM). EM II, enriched mantle II (see text). BE, bulk earth. Same symbols as for Figure 3. Solid diamond, Yamato Basin dredged lavas (Kaneoka, 1990); open circles, Miocene-Pliocene lavas from the backarc side of the Japan arc; open stars, Korea volcanics (Pouclet et al., unpublished data).

isotopic composition of the mantle source was weakly enriched to weakly depleted. The lower complex lavas are classified as backarc basin basalts. The trace-element and isotopic composition of the mantle source was moderately depleted. Magma genesis of the two series involved contribution of two mantle reservoirs: an enriched one of OIB-source type and a depleted one of MORB-source type with, in addition, a very slight participation of a crustal or subducted sediment component.

Age dating does not allow precise relative time setting of the two volcanic complexes that occurred between 22 and 17 Ma. However, the geochemical signatures of the two magmatic sequences are indicative of two distinct and successive events in the history of the Japan Sea opening: rifting and incipient spreading. In that case, the upper complex emplaced first and the lower complex intruded below the upper one. In a first stage, convective asthenospheric flow induced by subduction heated the continental margin behind the volcanic arc. Thinned lithosphere subsided in rift valleys, some evolving into marine basins. Partial melting of mantle produced tholeiite magma that intruded the rift floor. In a second stage, eastward retreat of the subducting slab enhanced tensional stress on the thermally weakened lithosphere and caused basin subsidence. Partial melting developed with increasing participation of the depleted upper mantle in the magma source, and backarc basalts invaded the basin floor. The Yamato spreading axis seems thus to have been located (Kimura et al., 1987). The Site 794 holes were drilled 25–30 km northeast of the axis. It is noteworthy that at Site 797, southwest of the Yamato Basin, two geochemically distinct volcanic sequences were found (Tamaki, Pisciotto, Allan, et al., 1990) with about the same compositions as the two complexes of Site 794 (Allan and Gorton, this volume) and with the same age range (Kaneoka et al., this volume). But the "backarc basalt" sequence, comparable with the lower complex, was settled above the "low-K tholeiite" sequence, comparable with the upper complex and with the tholeiites of the northwest Japan rifts (Tsuchiya, 1990), in a more conformable succession.

Neogene Magmatic History of the Yamato Basin

Data from the Site 794 igneous rocks yield basic information on the Neogene magmatic evolution of the Japan Sea area. Geochemical analyses and radiometric ages are available for Neogene volcanic rocks related or unrelated to the subduction process. They include dredged samples from the Yamato Bank and Basin (Kaneoka and Yuasa, 1988; Kaneoka, 1990; Kaneoka et al., 1990), lavas from the backarc side of the Japan arc (Uto et al., 1987; Iwamori, 1989, Tsuchiya, 1990), and lavas from the volcanic islands and the Korea margin (Nakamura et al., 1985; Yoon, 1987; Lee and Pouclet, 1988; Lee, 1989). The following synthesis of magmatic evolution is proposed:

24–20 Ma

In a pre-opening stage, calc-alkaline arc volcanism is documented from north Japan to Yamato Bank and to Pohang Basin in South Korea. The youngest andesites belonging to the remnant arc are dated from 20 Ma. Then a trenchward migration of the volcanic front to the east is explained by steepening of the subducting, older and colder Pacific Plate (Seno, 1985; Tatsumi et al., 1989).

22–17 Ma

The continental multiple rifting stage is characterized by continental tholeiites in north Japan (Akita-Yamagata rift zone) and in the Yamato Basin (Sites 794 and 797). Magmas were produced by partial melting of a DM and EM II-type mantle sources slightly contaminated by crustal components. Then, the multiple backarc spreading stage led to the formation of the Yamato and Japan Basins by fragmentation of the continental crust and isolation of continental blocks (Tamaki, 1988). This event is dated by marine transgressions in Japan and Korea at 17–16 Ma (Iijima and Tada, 1990). Magma compositions of the backarc basin basalts imply an increasing participation of the depleted MORB-like mantle source. Simultaneously, a complex horst and graben system developed in continental blocks giving rise to moderate volcanic activity of mafic to acidic composition.

17–10 Ma

In the post-opening stage, seamount volcanoes erupted on the floor of basins such as the Yamato Seamount chain, which is obviously in a near-ridge tectonic setting (Kimura et al., 1987). Chemical composition is moderately alkaline. The magmatic evolution is explained by lower degrees of partial melting and cooling of the mantle. At the same time, acidic volcanism took place in the continental crust rifted blocks: north Japan and Yamato bank (Pouclet et al., this volume).

10–0 Ma

Since late Miocene, scattered seamounts and some volcanic islands were built mainly on continental basement. From Pliocene to Pleistocene, island volcanism evolved to acidic composition with trachyte and phonolite lavas (Yoon, 1987; Lee, 1989). Similar alkaline volcanism took place on land on the backarc side of Japan and in central and north Korea. The alkaline and potassic chemical composition is explained by very low partial melting of OIB mantle source (Pouclet et al., unpublished data). One might expect the location of this alkaline volcanism is due to slower cooling of the continental basement of the backarc basin area.

ACKNOWLEDGMENTS

We thank the ODP chemistry technicians, Dawn J. Wright and Joan Perry, for their conscientious participation in the shipboard geochemical work, Ph. Vidal for the Sr and Nd isotopic measurements, and J.-C. Philippet for his technical assistance during mass spectrometry work. We are grateful to I. Kaneoka for basic discussions concerning the difficult problem of age dating of altered lavas; J. Allan, B. Cousens, and an anonymous reviewer for their constructive criticism of the original manuscript. This research was supported by a grant from CNRS, France.

REFERENCES

Bellon, H., Quoc Bun, N., Chaumont, J., and Philippet, J. C., 1981. Implantation ionique d'argon dans une cible support: application au traçage isotopique de l'argon contenu dans les minéraux et les roches. *C. R. Acad. Sci. Ser. 2, 292:977–980.*

Cabanis, B., and Lecolle, M., 1989. Le diagramme La/10-Y/15-Nb/8: un outil pour la discrimination des séries volcaniques et la mise en évidence des processus de mélange et/ou de contamination crustale. *C. R. Acad. Sci. Ser. 2,* 309:2023–2029.

Cassignol, C., David, B., and Gillot, P. Y., 1977. Contribution au dosage de l'argon dans l'échantillon de glauconite Gl-O. *Geostand. Newsl.,* 1:105–106.

Evensen, H. M., Hamilton, P. J., and O'Nions, R. K., 1978. Rare earth abundances in chondritic meteorites. *Geochim. Cosmochim. Acta,* 42:1199–1212.

Holm, P. E., 1985. The geochemical fingerprints of different tectono-magmatic environments using hygromagmatophile element abundances of tholeiitic basalts and basaltic andesites. *Chem. Geol.,* 51:303–323.

Iijama, A., and Tada, R., 1990. Evolution of Tertiary sedimentary basins of Japan in reference to opening of the Japan Sea. *J. Fac. Sci., Univ. Tokyo,* 22:121–171.

Ingle, J. C., Jr., Suyehiro, K., von Breymann, M. T., et al., 1990. *Proc. ODP, Init. Repts.,* 128: College Station, TX (Ocean Drilling Program).

Iwamori, H., 1989. Compositional zonation of Cenozoic basalts in the central Chugoku District: evidence for mantle upwelling. *Bull. Volcanol. Soc. Jpn.,* 34:105–123.

Kaneoka, I., 1990. Radiometric age and Sr isotope characteristics of volcanic rocks from the Japan Sea floor. *Geochem. J.,* 24:7–19.

Kaneoka, I., and Yuasa, M., 1988. ^{40}Ar-^{39}Ar age studies on igneous rocks dredged from central part of the Japan Sea. *Geochem. J.,* 22:195–204.

Kaneoka, I., Notsu, K., Takigami, Y., Fujioka, K., and Sakai, H., 1990. Constraints on the evolution of the Japan Sea based on ^{40}Ar-^{39}Ar ages and Sr isotopic ratios for volcanic rocks of the Yamato seamount chain in the Japan Sea. *Earth Planet. Sci. Lett.,* 97:211–225.

Kimura, M., Matsuda, T., Sato, H., Kaneoka, I., Tokuyama, H., Kuramoto, S., Oshida, A., Shimamura, K., Tamaki, K., Kinoshita, H., and Uyeda, S., 1987. Report on DELP 1985 cruises in the Japan Sea part VII: topography and geology of the Yamato Basin and its vicinity. *Bull. Earthq. Res. Inst., Univ. Tokyo,* 62:447–483.

Lee, J.-S., 1989. Pétrologie et relations structurales des volcanites crétacées à cénozoïques de la Corée du Sud: implications géodynamiques sur la marge Est-Eurasiatique [Ph.D. dissert.]. Univ. d'Orléans.

Lee, J.-S., and Pouclet, A., 1988. Le volcanisme néogène de Pohang (SE Corée), nouvelles contraintes géochronologiques pour l'ouverture de la Mer du Japon. *C. R. Acad. Sci. Ser. 2,* 307:1405–1411.

Mahood, G. A., and Drake, R. E., 1982. K-Ar dating young rhyolitic rocks: a case study of the Sierra La Primavera, Jalisco, Mexico. *Geol. Soc. Am. Bull.,* 93:1232–1241.

Meschede, M., 1986. A method of discriminating between different types of mid-oceanic ridge basalts and continental tholeiites with the Nb-Zr-Y diagram. *Chem. Geol.,* 56:207–218.

Nakamura, E., Campbell, I. H., and Sun, S., 1985. The influence of subduction processes on the geochemistry of Japanese alkaline basalts. *Nature,* 316:55–58.

Nohda, S., Tatsumi, Y., Otofuji, Y.-I., Matsuda, T., and Ishizaka, K., 1988. Asthenospheric injection and back-arc opening: isotopic evidence from northeast Japan. *Chem. Geol.,* 68:317–327.

Pearce, J. A., 1982. Trace element characteristics of lavas from destructive plate boundaries. *In* Thorpe, R. S. (Ed.), *Andesites:* New York (Wiley), 525–548.

Pearce, J. A., and Cann, J. B., 1973. Tectonic setting of basic volcanic rocks determined using trace element analyses. *Earth Planet. Sci. Lett.,* 19:290–300.

Pearce, J. A., and Norry, M. J., 1979. Petrogenetic implications of Ti, Zr, Y and Nb variations in volcanic rocks. *Contrib. Mineral. Petrol.,* 69:33–47.

Saunders, A. D., and Tarney, J., 1984. Geochemical characteristics of basaltic volcanism within back-arc basins. *In* Kokelaar, B. P., and Howells, M. F. (Eds.), *Marginal Basin Geology.* Geol. Soc. Spec. Publ. London, 16:59–76.

Seno, T., 1985. Age of subducting lithosphere and back-arc basin formation in the western Pacific since the middle Tertiary. *In* Nasu, N., et al. (Eds.), *Formation of Active Ocean Margins:* Tokyo (Terra Sci. Publ.), 469–481.

Steiger, R. H., and Jäger, E., 1977. Subcommission on geochronology convention on the use of decay constants in geo and cosmochronology. *Earth Planet. Sci. Lett.,* 26:359–362.

Tamaki, K., 1988. Geological structure of the Japan Sea and its tectonic implications. *Chishitsugaku Chosasho Geppo,* 39:269–365.

Tamaki, K., Pisciotto, K., Allan, J., et al., 1990. *Proc. ODP, Init. Repts.,* 127: College Station, TX (Ocean Drilling Program).

Tatsumi, Y., Otofuji, Y., Matsuda, T., and Nohda, S., 1989. Opening of the Sea of Japan back-arc basin by asthenospheric injection. *Tectonophysics,* 166:317–329.

Thompson, R. N., Morrison, M. A., Dickin, A. P., and Hendty, G. L., 1983. Continental flood basalts...arachnids rule OK? *In* Hawkesworth, C. J., and Norry, M. J. (Eds.), *Continental Basalts and Mantle Xenoliths:* Nantwich, U.K. (Shiva), 158–185.

Tsuchiya, N., 1990. Middle Miocene back-arc rift magmatism of basalt in the NE Japan arc. *Chishitsu Chosasho Geppo,* 41:473–505.

Uto, K., Hirai, H., Goto, K., and Arai, S., 1987. K-Ar ages of carbonate- and mantle nodule-bearing lamprophyres dykes from Shingu, central Shokoku, Southwest Japan. *Geochemical J.,* 21:283–290.

Uyeda, S., 1986. Facts, ideas and open problems on trench-arc-backarc systems. *In* Wezel, F.-C. (Ed.), *The Origin of Arcs:* Amsterdam (Elsevier), 435–460.

Wasserburg, G. J., Jacobsen, S. B., Depaolo, D. J., McCulloch, M. H., and Wen, T., 1981. Precise determination of Sm and Nd isotopic abundances in standard solutions. *Geochim. Cosmochim. Acta,* 45:2311–2323.

Wood, D. A., Joron, J. L., and Treuil, M., 1979. A re-appraisal of the use of trace elements to classify and discriminate between magma series erupted in different tectonic settings. *Earth Planet. Sci. Lett.,* 48:233–248.

Yoon, H. D., 1987. The geochemical characteristics and origin of alkaline magmas in the Ulleung Island, Korea [Ph.D. dissert.]. Seoul Univ., Korea.

Zindler, A., and Hart, S. R., 1986. Chemical geodynamics. *Annu. Rev. Earth Planet. Sci.,* 14:493–571.

Date of initial receipt: 8 April 1991
Date of acceptance: 2 October 1991
Ms 127/128B-197